Novel Techniques for Decomposing Diffuse Backgrounds

Brandon S. Hensley,[1, *] Vasiliki Pavlidou,[2, †] and Jennifer M. Siegal-Gaskins[3, 4, ‡]

[1]*Department of Astrophysical Sciences, Princeton University, Princeton, NJ 08544, USA*
[2]*Max-Planck Institute for Radioastronomy, 53121 Bonn, Germany*
[3]*California Institute of Technology, Pasadena, CA 91125, USA*
[4]*Center for Cosmology and Astro-Particle Physics,*
Ohio State University, Columbus, OH 43210, USA
(Dated: October 30, 2012)

The total anisotropy of a diffuse background composed of two or more sources, such as the *Fermi*-LAT–measured gamma-ray background, is set by the anisotropy of each source population and the contribution of each population to the total intensity. The total anisotropy as a function of energy (the anisotropy energy spectrum) will modulate as the relative contributions of the sources change, implying that the anisotropy energy spectrum also encodes the intensity spectrum of each source class. We develop techniques, applicable to any such diffuse background, for unraveling the intensity spectrum of each component source population given a measurement of the total intensity spectrum and the total anisotropy energy spectrum, without introducing *a priori* assumptions about the spectra of the source classes. We demonstrate the potential of these methods by applying them to example scenarios for the composition of the *Fermi*-LAT gamma-ray background consistent with current data and feasible within 10 years of observation.

I. INTRODUCTION

Diffuse emission, from radio to gamma-ray frequencies, encodes a wealth of information about fundamental physics, cosmology, and a variety of astrophysical systems. Prominent examples include the cosmic microwave background, a snapshot of the very early universe at microwave frequencies [1]; direct and reprocessed starlight between infrared and ultraviolet wavelengths, a record of the star formation history of the universe [2–4]; thermal emission from accretion processes in X-rays, which traces the growth of black holes through cosmic time [5]; and non-thermal emission in gamma rays from, e.g., blazars [6–8], star-forming galaxies [9], millisecond pulsars [10], and, possibly, annihilating or decaying dark matter [11–13].

Both the intensity spectrum and the degree of anisotropy of the diffuse signal have been successfully used to uncover valuable information about the physics and astrophysics of the processes and sources that are responsible for the diffuse emission in each waveband, the cosmic microwave background being the most celebrated example of both methods [e.g., 14, 15]. However, when more than one source class contributes to the diffuse emission, complications to such analyses arise. Traditionally, determining the individual contributions of source classes in a multi-population diffuse signal has relied on careful modeling and subtraction of intensity spectra [16]. This process is hindered by systematic uncertainties in the theoretical understanding of astrophysical source classes, which limit our ability to detect a possibly subdominant signal, especially one with unknown or poorly constrained properties.

In this work, we illustrate that a measurement of the anisotropy of a diffuse background at a fixed angular scale as a function of energy, when combined with the total intensity spectrum of the background, can be used to decouple the contributions to the background of each source population, thereby yielding an intensity spectrum for each source class. We focus here on applications to the isotropic diffuse gamma-ray background, as its large range of plausible compositions allows us to illustrate many of the techniques presented here.

The isotropic gamma-ray background (IGRB), the diffuse gamma-ray emission at energies above ~ 100 MeV that is isotropic on large angular scales, is one of the most promising observational targets for the discovery of new physics in this decade, such as a signature from dark matter annihilation or decay. Although the IGRB has been observed since the 1970s [17, 18], the Large Area Telescope (LAT) aboard the currently operational Fermi Gamma-Ray Space telescope (*Fermi* [19]) is improving both the energy range and the angular accuracy of these observations. The LAT also resolves more bright point sources than previous missions due to its increased sensitivity, providing valuable information about gamma-ray source populations via detected members. As a result, the LAT collaboration has reported a more precise measurement of the IGRB intensity spectrum [20], and for the first time has measured the small-scale anisotropy of the IGRB [21].

In addition to any possible exotic signal, confirmed astrophysical gamma-ray sources such as gamma-ray loud active galactic nuclei (blazars) and star-forming galaxies

---

*Electronic address: bhensley@astro.princeton.edu
†Current Address:Department of Physics, University of Crete, 71003 Heraklion, Greece
‡Einstein Fellow

are guaranteed to contribute significantly to the IGRB at some energy. Reference [22] showed that by combining the spectral and anisotropy properties of the IGRB, it is possible to identify the presence of a second, even sub-dominant, component, such as a signal from dark matter annihilation or decay, over a dominant, astrophysical contribution. We extend this approach by developing techniques that allow the intensity spectra of the individual components to be reconstructed without requiring a model or prediction for any of the contributions.

For diffuse backgrounds composed of emission from uncorrelated source populations, we show that under certain conditions, if the *intensity energy spectrum* (differential photon intensity as a function of energy) and the *anisotropy energy spectrum* (angular power at a fixed multipole as a function of energy) of the diffuse background are both measured with sufficient accuracy, the shape of the intensity energy spectrum of each component can be recovered; in some cases the absolute normalizations of the intensity spectra are also recoverable. Similarly, in some cases the amplitude of the angular power spectra of the individual components can also be determined. We discuss the conditions under which such decompositions are feasible, and demonstrate these novel techniques on plausible scenarios for the IGRB composition. Although our examples are restricted to the IGRB, the methods presented here can be applied to any diffuse background at any wavelength.

In §II we introduce the formalism common to all of the decomposition techniques. In §III we define IGRB component models and simulated observations used for the example scenarios. The details of each decomposition technique are described in §IV; example scenarios illustrating a subset of the techniques are also presented. We extend our approach to selected three-component scenarios in §V. We discuss the potential of these techniques for understanding gamma-ray source populations in §VI.

II. TWO-COMPONENT DECOMPOSITION: METHODS

The two properties of diffuse emission we will use are the differential intensity energy spectrum $I(E)$ (photons per area per time per solid angle per energy) and the angular power spectrum C_ℓ of a sky map of the intensity. The angular power spectrum is defined as $C_\ell = \langle |a_{\ell m}|^2 \rangle$, where $a_{\ell m}$ are the coefficients of the expansion of the intensity map in the basis of spherical harmonics. We also define the fluctuation angular power spectrum $\hat{C}_\ell \equiv C_\ell / I^2$, where I is the mean intensity of the emission with intensity angular power spectrum C_ℓ. Because $\hat{C}_\ell$ describes fluctuations in units of the mean, the fluctuation angular power at a fixed ℓ is energy-independent for a signal arising from a single population of sources with identical observer-frame intensity spectra. In the following we assume that each distinct component of the diffuse emission meets this criterion.

Variation between the source spectra of individual members of a population can result in fluctuation angular power which is energy dependent because the relative contributions of spectrally different sources within a population change with energy (e.g., harder sources contribute relatively more flux at high energies than at low energies). In addition, for cosmological source populations, energy-dependent fluctuation angular power can also arise due to redshifting of sharp features in the source spectra, such as line emission or abrupt cut-offs (see, e.g., [23, 24]).

In practice, if a component of the emission arises from a population of sources, we assume that the requirement that the single-population $\hat{C}_\ell$ is energy-independent is satisfied if the variation in the intensity spectra of individual members of the population is sufficiently small that the deviation of the fluctuation angular power from an energy-independent quantity is at a level smaller than the uncertainty on the anisotropy measured by a specific observation. We comment on the validity of this assumption in the context of the IGRB in §III.

Our approach exploits the energy independence of the single-component fluctuation angular power, and so it is convenient for us to work with $\hat{C}_\ell$. If we consider a scenario in which the diffuse emission is composed of emission from two spatially uncorrelated components with intensity spectra $I_1(E)$ and $I_2(E)$ and angular power spectra $C_{\ell,1}$ and $C_{\ell,2}$, then the total intensity is simply the sum of the two components,

$$I_{\text{tot}}(E) = I_1(E) + I_2(E). \quad (1)$$

The angular power spectrum of the total signal for uncorrelated components is the sum of the angular power spectra of the components,

$$C_{\ell,\text{tot}}(E) = C_{\ell,1}(E) + C_{\ell,2}(E). \quad (2)$$

Rewritten in terms of the fluctuation angular power,

$$\hat{C}_{\ell,\text{tot}}(E) = \left(\frac{I_1(E)}{I_{\text{tot}}(E)} \right)^2 \hat{C}_{\ell,1} + \left(\frac{I_2(E)}{I_{\text{tot}}(E)} \right)^2 \hat{C}_{\ell,2}. \quad (3)$$

This is the fluctuation anisotropy energy spectrum for the case we consider. In the following we will always use the term "anisotropy energy spectrum" to refer to the *fluctuation* angular power of the total emission as a function of energy.

With sufficient photon statistics, I_{tot} and $\hat{C}_{\ell,\text{tot}}$ can be determined at each energy from observations. If there is a way to also determine $\hat{C}_{\ell,1}$ and $\hat{C}_{\ell,2}$ from the data, we can solve Eqs. (1) and (3) for I_1 and I_2:

$$I_1 = I_{\text{tot}} \left(\frac{\hat{C}_{\ell,2} \pm \sqrt{\hat{C}_{\ell,1}\hat{C}_{\ell,\text{tot}} + \hat{C}_{\ell,2}\hat{C}_{\ell,\text{tot}} - \hat{C}_{\ell,1}\hat{C}_{\ell,2}}}{\hat{C}_{\ell,1} + \hat{C}_{\ell,2}} \right) \quad (4)$$

$$I_2 = I_{\text{tot}} \left(\frac{\hat{C}_{\ell,1} \mp \sqrt{\hat{C}_{\ell,1}\hat{C}_{\ell,\text{tot}} + \hat{C}_{\ell,2}\hat{C}_{\ell,\text{tot}} - \hat{C}_{\ell,1}\hat{C}_{\ell,2}}}{\hat{C}_{\ell,1} + \hat{C}_{\ell,2}} \right). \quad (5)$$

TABLE I: Summary of two-component decomposition techniques.

Method	Observational Signature	Inferred Properties of Components	Intensity Normalization Recovered?	Fluctuation Angular Power Recovered?
Double plateau	Plateaus at both high and low energies observed in anisotropy energy spectrum	One source dominant in anisotropy at low energies, other source dominant at high energies	Yes	Yes
Low-Anisotropy Plateau	Anisotropy energy spectrum rises from (falls to) a low-anisotropy plateau at low (high) energy	Source that is subdominant in intensity is much more anisotropic than the dominant source	No	No
High-Anisotropy Plateau	Anisotropy energy spectrum falls from (rises to) a high-anisotropy plateau at low (high) energy	Source that is subdominant in intensity is much less anisotropic than the dominant source	Yes	No
Known Zero-Anisotropy Component	None; requires *a priori* knowledge that one of the two components is isotropic	One source is completely isotropic	No	No
Minimum	Minimum observed in the anisotropy energy spectrum	Both source components have comparable intensity and anisotropy such that Eq. 20 is satisfied at some energy	Yes	Yes
Multiple-ℓ Measurements	Two distinct anisotropy energy spectra can be obtained at two different ℓ	$\hat{C}_\ell$ is a function of ℓ for at least one source such that two distinct anisotropy energy spectra can be obtained at different ℓ	Yes	Yes

If there is an energy $\sim E_0$ around which only one component is expected to contribute to the total intensity (i.e., an energy range around E_0 where $I_2(E_0)/I_{\rm tot}(E_0) \approx 0$), the anisotropy energy spectrum will be flat over this energy range. Then from Eq. (3) we immediately obtain $\hat{C}_{\ell,1} = \hat{C}_{\ell,{\rm tot}}(E_0)$ from the anisotropy of this baseline. A similar flat baseline could result if two source classes have the same spectral shape over an energy range, but such a scenario is unlikely for the source classes considered here. *In each of the following cases, we will assume either that we can obtain the $\hat{C}_\ell$ of one of the two source classes in this way, or that one source class is known to have $\hat{C}_\ell \simeq 0$.*

We discuss six distinct two-component decomposition techniques below. Some of them allow us to extract the component intensity spectra, while others only allow us to derive the *shapes* of one or both intensity spectra up to unknown normalization constants. Some of the techniques also yield measurements of the fluctuation angular power spectra of each component source population. Table I gives a summary of these techniques and their applicability conditions. We emphasize that in all cases we make the following three assumptions: (1) the diffuse background is composed of emission from uncorrelated

source classes, (2) the fluctuation angular power of each individual component is independent of energy, and (3) the fluctuation angular power of one component can be directly measured from the data at some energy or is known to be negligibly small.

III. PARAMETERS OF EXAMPLE SCENARIOS

A. IGRB Component Models

To illustrate the decomposition techniques, we apply them to example scenarios that could be measured by the *Fermi*-LAT within 10 years of observation time. Each scenario is a two-component IGRB model consistent with current observations of the measured IGRB intensity energy spectrum [20] and the measurement of the IGRB anisotropy energy spectrum [21]. In particular, we consider a power law component with slope and fluctuation anisotropy that describes the IGRB well at low energies but that may break at high energies, as well as a Galactic dark matter annihilation component with one of two benchmark spectra (annihilation to a $\tau^+\tau^-$ or $b\bar{b}$ final state).

The power law component encapsulates likely contributions from several source classes such as blazars, but we assume, in accord with the data, that this emission can be characterized by a single $\hat{C}_\ell$. The adopted $\hat{C}_\ell$ in this work differs from that derived in [21] as we use the intensities reported by [20] rather than those used in the anisotropy analysis, which were subjected to less cleaning. As this cleaning likely removed only isotropic contamination, we expect that the angular power C_P derived in [21] also describes the IGRB of [20], and thus we check for consistency with C_P only.

Although we do not consider them explicitly in our example scenarios, other known gamma-ray source populations which may contribute significantly to the intensity and/or anisotropy of the IGRB at some energies include star-forming galaxies [9, 25–29], gamma-ray loud radio galaxies [30] and Galactic millisecond pulsars [10, 31].

For source classes relevant for the IGRB, the three assumptions stated above, which are necessary to implement our methods, are very likely to be valid. While all cosmological populations will generally trace large-scale structure, on the small angular scales considered in the *Fermi* LAT anisotropy analysis [21] we do not expect strong spatial correlations between, e.g., blazars and extragalactic dark matter [32], and naturally the angular distribution of any Galactic source population is entirely uncorrelated with that of any extragalactic population. For these source classes, the variation between observer-frame source spectra within the population is likely to be sufficiently small (or zero, in the case of Galactic dark matter annihilation or decay) to induce at most a mild energy dependence in the fluctuation angular power, although we caution that a careful investigation of the expected magnitude of this effect is needed. Furthermore, most expected cosmological contributors to the IGRB are not expected to exhibit features in their spectra which are sharp enough to lead to significant energy dependence of the fluctuation angular power due to redshifting. Although in some dark matter models sharp features are present in the photon spectra, in many scenarios the Galactic dark matter signal is expected to dominate over the extragalactic signal in both intensity and anisotropy, so any energy dependence in the fluctuation angular power of the extragalactic dark matter component would likely have a subdominant effect. Finally, the expected contributors to the IGRB have different spectral shapes, and consequently it is not unlikely that at certain energies all but one component will supply a negligible contribution, in which case the fluctuation angular power of the dominant component could be measured as described in the previous section.

The level of the blazar contribution to the IGRB is uncertain, with different calculations spanning a large range of possibilities (e.g., [6–8, 33–35]). The strongest bounds on the contribution of blazars to the intensity of the IGRB have been obtained by requiring that the adopted model for the blazar population does not exceed the measured IGRB anisotropy [34, 35]; these bounds limit the blazar IGRB intensity contribution to $\lesssim 20\%$ in the 1–10 GeV band. The spectral shape of the blazar contribution is dependent primarily on the distribution of blazar spectral indices in the gamma-ray range [36]. Since BL Lac–type blazars and flat-spectrum radio quasars (FSRQs), the two largest subclasses of blazars, generally have different spectral properties, the shape of the collective intensity spectrum depends on the relative abundances of these two subclasses in the unresolved blazar population, which is uncertain due to the difficulties in obtaining BL Lac redshifts and assessing the prevalence of BL Lacs in the high-redshift universe [6]. Additional uncertainties enter through considerations regarding the fraction of blazars with spectral breaks [37].

Source intensity spectra at energies above a few tens of GeV from high-redshift populations are attenuated by interactions with the EBL, which consists of infrared, optical, and ultraviolet photons primarily from direct and reprocessed starlight throughout cosmic history. While *Fermi* observations have produced constraints on models of the EBL [38, 39], the details remain quite uncertain [3, 40–42] . In some of the models we consider, we use a broken power-law model for the non-dark-matter emission, which can act as a proxy for EBL attenuation as well as for accounting for the intrinsic properties of the emitting sources.

We assume an anisotropy for our composite power law consistent with observations rather than tying it to models of a given source class. A significant contribution to the anisotropy is expected to come from unresolved blazars. The anisotropy properties of the blazar contribution to the background are generally dependent on the details of the blazar luminosity function, and therefore similarly uncertain as the overall amplitude of the collective blazar intensity. The derived anisotropy of the IGRB is comparable to the level of blazar fluctuation anisotropy predicted by theoretical work (see, e.g., [32]), though blazars are expected to be too anisotropic to contribute the entire IGRB [34, 35].

For the dark matter component in our example scenarios, we model the emission from pair annihilation of WIMP dark matter particles in Galactic subhalos. We consider the photon intensity spectra given in [43] produced by annihilation into two benchmark final states: (1) $b\bar{b}$, which generates a relatively soft continuum photon spectrum primarily from the decay of neutral pions produced by the hadronization of quark jets, and (2) $\tau^+\tau^-$, which produces a harder photon spectrum due to a significant contribution from final state radiation associated with the production of charged leptons. We choose values of the annihilation cross section between the canonical value for a thermal relic $\langle \sigma v \rangle_0 = 3.0 \times 10^{26} \, \mathrm{cm}^3\mathrm{s}^{-1}$ [44] (see also [45]) and 33 times that value. Different constraints on dark matter models can be obtained under different assumptions for various targets, (e.g., [46–52]). The fluctuation anisotropy from dark matter annihilation, which is determined exclusively by the spatial distribution of the dark matter, has been predicted for annihi-

lation in Galactic dark matter subhalos by Refs. [53–56]. We present three models with a dark matter component: one that falls within the typical predictions for the dark matter anisotropy and two models that do not. However, we emphasize that the model parameters adopted for each example scenario were chosen to be illustrative of the decomposition methods rather than to represent the most plausible compositions of the *Fermi*-LAT IGRB.

B. Error Analysis

We compute error bars for the example IGRB intensity and anisotropy energy spectra assuming observations with the *Fermi*-LAT. The 1σ error bars for the total fluctuation anisotropy in each energy bin were computed using the formula [57]:

$$\Delta \hat{C}_\ell = \sqrt{\frac{2}{(2\ell + 1)\,\Delta\ell f_{sky}}} \left(\hat{C}_\ell + \frac{\hat{C}_N}{W_\ell^2} \right) \qquad (6)$$

where $\hat{C}_\ell$ is the total fluctuation angular power spectrum, $\Delta\ell$ is the width of the multipole bin, f_{sky} is the fraction of the sky used to calculate the angular power spectrum, $\hat{C}_N = (4\pi f_{sky}/N_\gamma)$ is the power spectrum of the photon noise associated with the total measured emission, with N_γ the total number of photons collected during the observation period in the sky region analyzed, and W_ℓ is the beam window function of the instrument.

We approximate the PSF of the LAT as a circular Gaussian beam with energy-dependent width $\sigma_b(E)$, determined from the 68% containment angle radius reported in the P7_V6 performance curves [61], so $W_\ell = \exp\left(-\ell^2\sigma_b^2/2\right)$, which is the window function of a Gaussian beam of width σ_b. We evaluate σ_b at the log center of the energy bin. For the example scenarios, we show anisotropy energy spectra at $\ell = 175$, and take $\Delta\ell = 50$, choices made to ease comparison with the results reported in the *Fermi* anisotropy analysis [21] which used $\Delta\ell = 50$ and focused on the Poisson angular power measured at $\ell \gtrsim 150$ to limit contamination from Galactic diffuse emission.

Following the *Fermi* anisotropy analysis, we assume a sky fraction $f_{sky} = 0.32$ is used to perform the anisotropy and intensity measurements, i.e., a large fraction of the sky is masked. We take the field of view of the LAT to be $\Omega = 2.4$ sr, and approximate the energy-dependent effective area of the LAT from the reported performance curves. For a specified all-sky observation time t_{obs}, we calculate the number of photons detected outside the mask to be $N_\gamma = \int_{E_{\min}}^{E_{\max}} dE\, \frac{dI}{dE}\, A_{\text{eff}}(E)\, \Omega\, f_{sky}\, t_{obs}$, where $\frac{dI}{dE}$ is the total (energy-dependent) differential intensity of the IGRB, A_{eff} is the energy-dependent effective area of the instrument, and we have assumed observations in all-sky survey mode and uniform sky exposure.

The errors on the intensity energy spectra represent the Poisson noise associated with the number of photons collected in each energy bin, as well as an assumed 20% uncertainty on the effective area of the instrument as estimated from the performance curves; we note that the uncertainty on the effective area does not contribute to the uncertainty in the fluctuation angular power spectra since normalizing intensity fluctuations to the mean map intensity removes the effective area from the calculation. For the all-sky observation time of 10 years assumed in the examples presented in this work, we find that for the adopted energy binning, the uncertainty in A_{eff} dominates the error bars on the intensity spectra up to a few hundred GeV for all of the scenarios considered here, resulting in relatively uniform error bars as a function of energy.

The errors on the simulated intensity and anisotropy spectra can be propagated through the decomposition equations, enabling calculation of error bars for the decomposed intensity spectra. Often, the $\hat{C}_\ell$ of one source class must be obtained from a flat baseline in the anisotropy energy spectrum over the energies where that source class dominates the anisotropy. An estimate for the $\hat{C}_\ell$ of such a source class can be obtained by taking the weighted mean of the baseline points with error equal to the weighted error of the mean. The decomposed intensity spectra can then be written in terms of quantities for which a mean and error bar can be computed. The 1σ and 3σ confidence intervals are determined via Monte Carlo.

IV. TWO-COMPONENT DECOMPOSITION: APPLICATIONS

The formalism for each of the six two-component decomposition techniques summarized in Table I is given in the following subsections.

A. Double Plateau

As previously described, we can infer the value of $\hat{C}_{\ell,1}$ by observing a flat baseline (plateau) in the anisotropy energy spectrum at either low or high energies. In the event that we observe a second such plateau in the anisotropy energy spectrum (Fig. 1) with amplitude either above or below the level of the first plateau $\hat{C}_{\ell,1}$ (*i.e.* where $I_1 \ll I_2$), we can obtain a value for $\hat{C}_{\ell,2}$. In this case Eqs. 4 and 5 for the intensity spectra of the two components can be solved directly. This is a *double plateau decomposition*, and corresponds to the case that one of the components dominates the anisotropy at low energies, while the other dominates the anisotropy at high energies. In this case we assume the anisotropy energy spectrum increases or decreases monotonically between the two plateaus; the case of local extrema is discussed in the case of a minimum decomposition in §IV E. A double plateau is a particularly ideal case because the input

spectra can be derived exactly, without making any assumptions about the relative contributions of the source classes to either the total intensity or anisotropy that cannot be inferred directly from the observed spectra.

As an example scenario, shown in Fig. 1, we choose $m_{\rm DM} = 300$ GeV, $\langle \sigma v \rangle = 20 \langle \sigma v \rangle_0$, and annihilation into $\tau^+ \tau^-$ for the dark matter intensity spectrum, and adopt a broken power law for the remaining intensity spectrum. The anisotropies were taken to be $\hat{C}_\ell = 1.2 \times 10^{-4}$ sr, and $\hat{C}_\ell = 5 \times 10^{-3}$ sr for the broken power law and dark matter signals, respectively. Because the anisotropy energy spectrum is still rising slightly between the last two data points, the estimate for the $\hat{C}_\ell$ of the dark matter component will be biased low, thus slightly biasing the decomposed spectra away from the true value.

B. Low-Anisotropy Plateau

We now consider a scenario in which a low-anisotropy plateau is measured in the anisotropy energy spectrum at low or high energies, and the anisotropy rises from the plateau at low energies or falls to the plateau at high energies. This corresponds to a case where the component subdominant in intensity at the plateau has a much higher anisotropy,

$$\hat{C}_{\ell,1} \ll \hat{C}_{\ell,2} = \Lambda \hat{C}_{\ell,1} \tag{7}$$

with $\Lambda \gg 1$.

In this case, Eq. (3) can be written as

$$\hat{C}_{\ell,\rm tot} = \left(1 - \frac{I_2}{I_{\rm tot}}\right)^2 \hat{C}_{\ell,1} + \left(\frac{I_2}{I_{\rm tot}}\right)^2 \Lambda \hat{C}_{\ell,1} \tag{8}$$

or

$$\frac{\hat{C}_{\ell,\rm tot}}{\hat{C}_{\ell,1}} = 1 - 2\frac{I_2}{I_{\rm tot}} + (1 + \Lambda)\left(\frac{I_2}{I_{\rm tot}}\right)^2. \tag{9}$$

Now we define $x(E) = I_2/I_{\rm tot}$ and $\omega(E) = \hat{C}_{\ell,\rm tot}/\hat{C}_{\ell,1} - 1$, which can be determined by observations at each energy. Then we have

$$(1 + \Lambda)x^2 - 2x - \omega = 0 \tag{10}$$

with solution

$$x = \frac{1 \pm \sqrt{1 + (1+\Lambda)\omega}}{1 + \Lambda}. \tag{11}$$

Since $\Lambda \gg 1$, as long as $\omega > 1$ we can approximate this by

$$x \approx \frac{1 \pm \sqrt{(1+\Lambda)\omega}}{1 + \Lambda} \approx \frac{\sqrt{\omega}}{\sqrt{1+\Lambda}}. \tag{12}$$

where we have selected the $+$ solution since x is a nonnegative quantity. Since ω is an observable, it is always possible to determine whether the $\omega > 1$ condition holds.

The shape of the subdominant spectrum can thus be derived up to a multiplicative constant.

As an example scenario, shown in Fig. 2, we choose a dark matter particle with $m_{\rm DM} = 1000$ GeV that annihilates to $b\bar{b}$ with $\langle \sigma v \rangle = 33 \langle \sigma v \rangle_0$ and a broken power law component to the intensity spectrum. We set the fluctuation angular power to $\hat{C}_\ell = 1 \times 10^{-4}$ sr for the broken power law component, and $\hat{C}_\ell = 2.5 \times 10^{-3}$ sr for dark matter.

C. High-Anisotropy Plateau

If a high-anisotropy plateau is measured in the anisotropy energy spectrum at low or high energies, and the anisotropy falls from the plateau at low energies or rises to the plateau at high energies, then a less anisotropic source must be making an increasing contribution to the background at energies far from the plateau. We now consider this scenario, corresponding to the case that one component is *everywhere* dominant in the intensity,

$$I_1 > I_2 \tag{13}$$

and also more anisotropic

$$\hat{C}_{\ell,1} \gg \hat{C}_{\ell,2}. \tag{14}$$

In this case, Eq. 3 can be approximated by

$$\hat{C}_{\ell,\rm tot} \approx \left(\frac{I_1}{I_{\rm tot}}\right)^2 \hat{C}_{\ell,1}. \tag{15}$$

Immediately then we have

$$I_1 \approx I_{\rm tot}\sqrt{\frac{\hat{C}_{\ell,\rm tot}}{\hat{C}_{\ell,1}}} \tag{16}$$

and

$$I_2 \approx I_{\rm tot}\left(1 - \sqrt{\frac{\hat{C}_{\ell,\rm tot}}{\hat{C}_{\ell,1}}}\right). \tag{17}$$

The assumption that the higher anisotropy source is dominant must be satisfied at the energies where the high-anisotropy plateau is measured. Each subsequent point moving away from the plateau in energy will yield a value for the fractional contribution of the subdominant source via the ratio of Eqns. 16 and 17. Therefore, the appropriateness of the assumption that the anisotropic source is dominant can always be verified. This decomposition yields both the shape of the intensity spectra as well as their normalizations.

As an example scenario, shown in Fig. 3, we choose a dark matter particle with $m_{\rm DM} = 200$ GeV that annihilates to $\tau^+ \tau^-$ with $\langle \sigma v \rangle = 6.7 \langle \sigma v \rangle_0$ and a component with a power law intensity spectrum. We set the fluctuation angular power to $\hat{C}_\ell = 1.2 \times 10^{-4}$ sr for the power
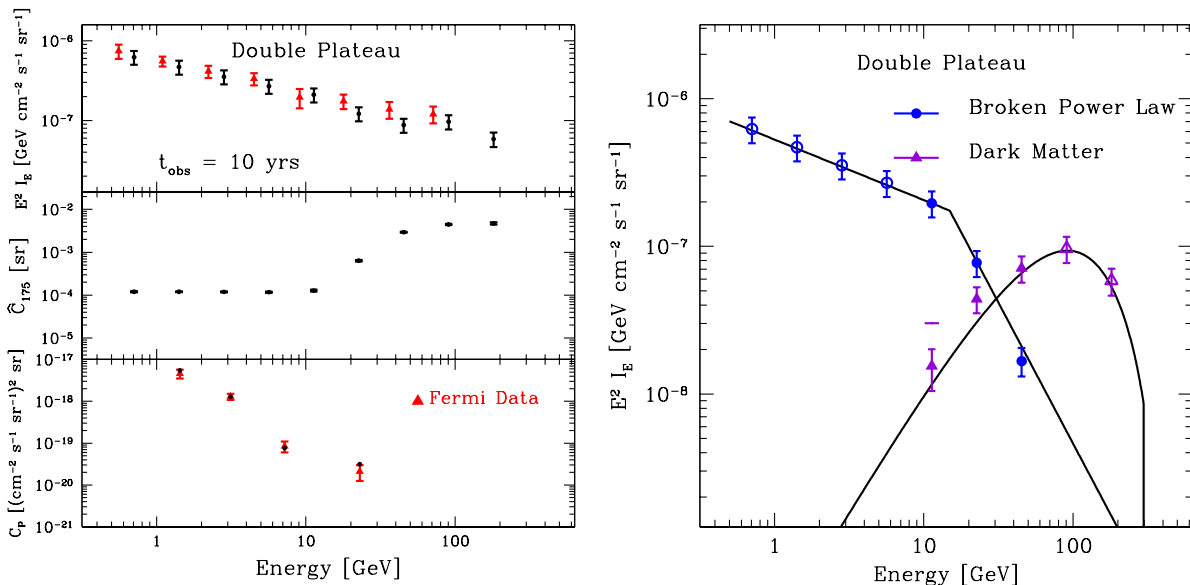
FIG. 1: Example double plateau decomposition. *Left:* Total IGRB intensity (top), anisotropy energy spectrum (middle), and angular power C_P (bottom). Energy bins are equally spaced in log space, and all quantities are reported at the log center of the energy bin. Error bars assume $t_{obs} = 10$ years of *Fermi*-LAT observations in sky-survey mode. If a data point is within 3σ of zero, we place a 3σ upper limit bar in addition to the 1σ error bars. Red triangles indicate the *Fermi* IGRB intensity and angular power measurements. The dark matter intensity spectrum corresponds to a $m_{DM} = 300$ GeV particle annihilating to $\tau^+\tau^-$. *Right:* The decomposed intensity energy spectrum of the power law component (blue circles) and dark matter annihilation (purple triangles) recovered using the plateau technique. The baseline points (open plot symbols) from which $\hat{C}_{\ell,1}$ and $\hat{C}_{\ell,2}$ were determined were not decomposed. Each component's input intensity spectrum is overlaid in black.

law component, and $\hat{C}_\ell = 5 \times 10^{-6}$ sr for dark matter. These parameters are consistent with current observational and theoretical constraints on the IGRB intensity, anisotropy, and dark matter properties.

D. Known Zero-Anisotropy Component

If one of the components of a two-component background is completely isotropic, then Eq. 3 becomes:

$$\hat{C}_{\ell,tot} = \left(\frac{I_1}{I_{tot}}\right)^2 \hat{C}_{\ell,1} \qquad (18)$$

which may be rewritten simply as

$$I_1 = I_{tot}\sqrt{\hat{C}_{\ell,tot}/\hat{C}_{\ell,1}}. \qquad (19)$$

Thus, in this case the shape of the spectrum of the component with nonzero anisotropy can be determined up to a multiplicative constant by measuring $I_{tot}(E)$ and $\hat{C}_{\ell,tot}(E)$. This technique is a special case of the high-anisotropy plateau where Eqns. 16 and 17 hold exactly, regardless of which source is dominant. We emphasize that this method requires *a priori* knowledge that a zero-anisotropy component exists, but does not require knowledge of the shape or normalization of its intensity spectrum.

To demonstrate such a decomposition, as shown in Fig. 4, we analyze the intensity and anisotropy data as measured by *Fermi*-LAT; note that the measured anisotropy energy spectrum is consistent with no energy dependence.

The decomposition presented in Fig. 4 yields spectra with slope consistent with the slope of the composite IGRB. This decomposition technique recovers the shape but not the normalization of the intensity spectrum of the anisotropic component, hence the normalizations shown in Fig. 4 are arbitrary. We caution the reader that this is not a definitive decomposition of the *Fermi*-LAT IGRB due to uncertainty in matching the intensity and anisotropy measurements from two different studies, and in addition it is subject to the assumption that a zero-anisotropy component exists in the measured IGRB.

E. Minimum

Assuming $\hat{C}_{\ell,1}$ can be inferred from the data by measuring a plateau in the anisotropy energy spectrum, an additional way to determine $\hat{C}_{\ell,2}$ and decompose the observed intensity spectrum exists if a local minimum is observed in the anisotropy energy spectrum. The condition for observing a minimum in the anisotropy energy spectrum can be obtained by differentiating Eq. (3) with
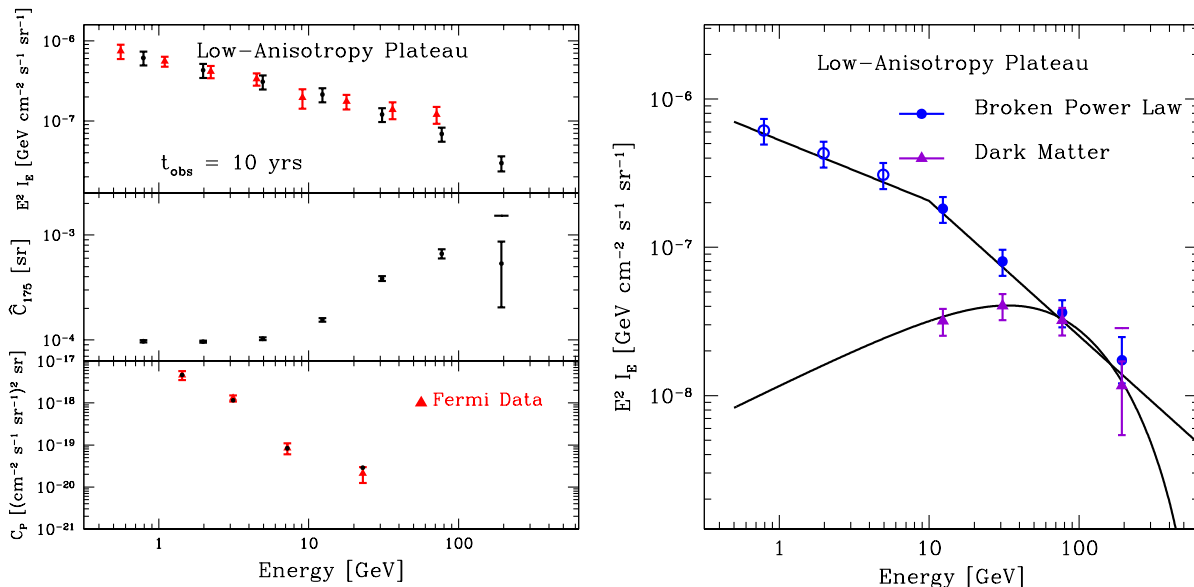
FIG. 2: Example low-anisotropy plateau decomposition. *Left:* Total IGRB intensity (top), anisotropy energy spectrum (middle), and angular power C_P (bottom). Energy bins are equally spaced in log space, and all quantities are reported at the log center of the energy bin. Error bars assume $t_{\rm obs} = 10$ years of *Fermi*-LAT observations in sky-survey mode. If a data point is within 3σ of zero, we place a 3σ upper limit bar in addition to the 1σ error bars. In this scenario the IGRB is composed of emission from a broken power law component and Galactic dark matter annihilation. The dark matter intensity spectrum corresponds to a $m_{\rm DM} = 1000$ GeV particle annihilating to $b\bar{b}$. *Right:* The decomposed intensity energy spectra of the power law component (blue circles) and dark matter annihilation (purple triangles) are recovered using the low-anisotropy plateau technique. The baseline points at low energy (open plot symbols) from which $\hat{C}_{\ell,1}$ was determined were not decomposed. Each component's input intensity spectrum is overlaid in black. Red triangles indicate the *Fermi* IGRB intensity and angular power measurements. Note that this method recovers the normalizations of each component's intensity spectrum up to a multiplicative constant; the constant has been set to the true value to facilitate comparison with the input spectral shapes.

respect to energy. We find that a minimum occurs when

$$\hat{C}_{\ell,2} \left(\frac{I_1(E_{\rm min})}{I_{\rm tot}(E_{\rm min})} - 1 \right) + \hat{C}_{\ell,1} \frac{I_1(E_{\rm min})}{I_{\rm tot}(E_{\rm min})} = 0 \,. \quad (20)$$

At the energy at which the local minimum occurs $E_{\rm min}$, we can simultaneously solve this equation with Eq. 1 at the same energy to obtain

$$\hat{C}_{\ell,2} = \frac{\hat{C}_{\ell,1}\hat{C}_{\ell,{\rm tot}}(E_{\rm min})}{\hat{C}_{\ell,1} - \hat{C}_{\ell,{\rm tot}}(E_{\rm min})}. \quad (21)$$

Substituting this relation into Eqs. 4 and 5 completely determines the intensity energy spectrum for both source classes. In this case, a *minimum decomposition* is possible. For appropriate levels of anisotropy and fractional contribution to the background, Eq. 3 states that the total anisotropy can be less than the anisotropy of either source class. Indeed, the minimum will exist only if there is an energy at which $I_1\hat{C}_{\ell,1} = I_2\hat{C}_{\ell,2}$, and this requirement will always produce a minimum rather than a maximum in the total anisotropy since

$$\left. \frac{d^2\hat{C}_{\ell,{\rm tot}}}{dE^2} \right|_{E_{\rm min}} = 2 \left(\frac{d}{dE}\frac{I_1}{I_{\rm tot}} \right)^2 \left(\hat{C}_{\ell,1} + \hat{C}_{\ell,2} \right) \quad (22)$$

is non-negative. It also implies that a component which is always subdominant cannot be decomposed using this technique if its angular power is also smaller than that of the dominant component. A second caveat of this method is that a minimum can also occur when $\frac{d}{dE}\left(\frac{I_2}{I_{\rm tot}} \right) = 0$, which does not yield a constraint on $\hat{C}_{\ell,2}$. This occurs when a low anisotropy component transitions from contributing an increasing fraction of the total intensity to contributing a decreasing fraction of the total intensity. Thus, the anisotropy of the resulting minimum must be intermediate between the anisotropy of each source class. On the other hand, the decomposition minimum occurs at an anisotropy below that of either source class. Hence, in practice, the two types of minima may be distinguished if the anisotropy energy spectrum is observed to take on values both above and below an observed baseline, in which case it must be a decomposition minimum.

The biggest challenge in the applicability of this technique is that the uncertainties associated with an observed anisotropy energy spectrum will often be too high to allow a minimum to be measured. The depth of the minimum is given by the ratio of $\hat{C}_{\ell,{\rm tot}}$ at the minimum and the lesser of $\hat{C}_{\ell,1}$ and $\hat{C}_{\ell,2}$. By rearranging Eq. 21
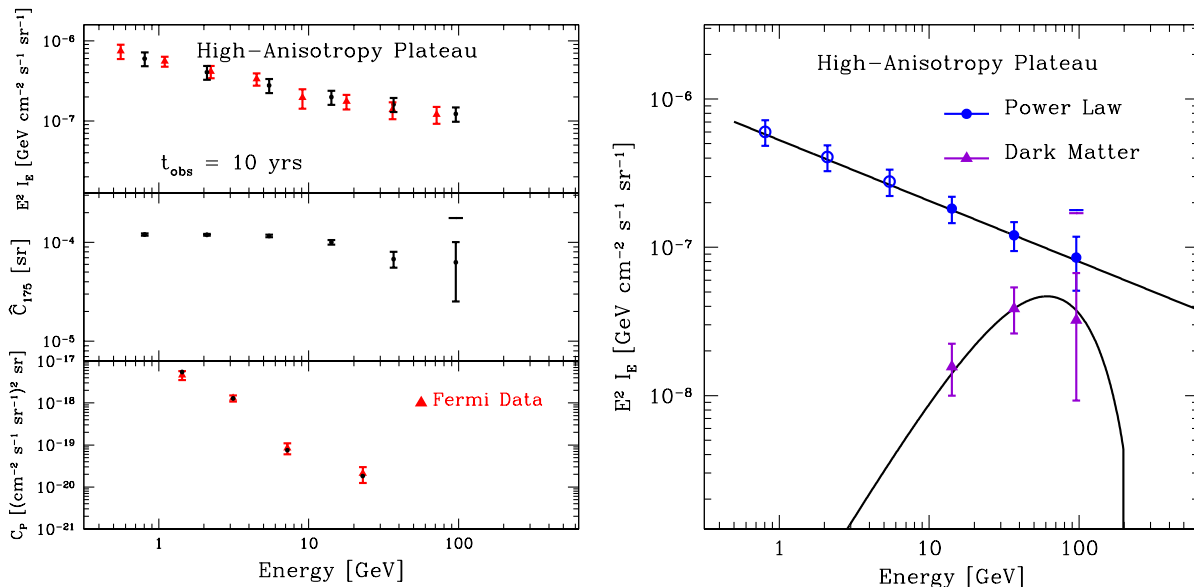
FIG. 3: Example high-anisotropy plateau decomposition. *Left:* Total IGRB intensity (top), anisotropy energy spectrum (middle), and angular power C_P (bottom). Energy bins are equally spaced in log space, and all quantities are reported at the log center of the energy bin. Error bars assume $t_{\rm obs} = 10$ years of *Fermi*-LAT observations in sky-survey mode. If a data point is within 3σ of zero, we place a 3σ upper limit bar in addition to the 1σ error bars. In this scenario the IGRB is composed of emission from a power-law component and Galactic dark matter annihilation. The dark matter intensity spectrum corresponds to a $m_{\rm DM} = 200$ GeV particle annihilating to $\tau^+\tau^-$. *Right:* The decomposed intensity energy spectra of the power law component (blue circles) and dark matter annihilation (purple triangles) recovered using the low-anisotropy plateau technique. The baseline points at low energy (open plot symbols) from which $\hat{C}_{\ell,1}$ was determined were not decomposed. Each component's input intensity spectrum is overlaid in black. Red triangles indicate the *Fermi* IGRB intensity and angular power measurements.

and assuming $\hat{C}_{\ell,1} > \hat{C}_{\ell,2}$ we obtain

$$\frac{\hat{C}_{\ell,\rm tot}}{\hat{C}_{\ell,2}} = \frac{\hat{C}_{\ell,1}}{\hat{C}_{\ell,1} + \hat{C}_{\ell,2}} \qquad (23)$$

Thus the depth of the minimum varies between 0.5 and 1 times $\hat{C}_{\ell,1}$, with the largest depth occurring for $\hat{C}_{\ell,1} = \hat{C}_{\ell,2}$. For instance, although the example given in §IV B (low-anisotropy plateau) in principle exhibits a local minimum in the anisotropy energy spectrum, the depth of this minimum would be very small and thus challenging to measure observationally.

However, this does not mean that likely two-component scenarios for the IGRB that would allow a minimum decomposition do not exist. One such scenario can be envisioned if blazars typically exhibit spectral breaks. In combination with the different population-average spectral indices of BL Lacs and FSRQs, this could lead to a scenario in which over a certain energy range the IGRB is composed of emission from two source classes (BL Lacs and FSRQs), and the dominant contributor to the intensity transitions between the source classes at a few GeV (see, e.g., Fig. 3 of [37]). If BL Lacs and FSRQs have approximately equal levels of fluctuation angular power (not unlikely, as *Fermi* has resolved comparable numbers of sources in each of the two

classes), the minimum in the anisotropy energy spectrum would appear around the transition energy of a few GeV, where photon statistics would be fairly large and thus may allow a measurement of the minimum.

We note that by examining the conditions under which a minimum occurs, we can also better understand the degeneracy in choice of sign in Eqs. 4 and 5. By rearranging Eq. 5, which gives

$$I_2\hat{C}_{\ell,2} - I_1\hat{C}_{\ell,1} = \qquad (24)$$
$$\pm I_{\rm tot}\sqrt{\hat{C}_{\ell,1}\hat{C}_{\ell,\rm tot} + \hat{C}_{\ell,2}\hat{C}_{\ell,\rm tot} - \hat{C}_{\ell,1}\hat{C}_{\ell,2}}$$

we see that the proper sign is determined based upon the sign of $I_2\hat{C}_{\ell,2} - I_1\hat{C}_{\ell,1}$. As the relative contributions of the two source classes fluctuate, however, this quantity can go from positive to negative, forcing us to switch the choice of signs when this happens. Notably, a sign change would have to occur when $I_1\hat{C}_{\ell,1} = I_2\hat{C}_{\ell,2}$, precisely when $\hat{C}_{\ell,\rm tot}$ is minimized. Indeed, since $I_2/I_{\rm tot}$ is changing through the minimum, the sign *must* change at every minimum with the only exception being when $I_2/I_{\rm tot}$ is simultaneously minimized or maximized, which does not happen in general. Consequently, no single choice of signs describes the entire spectrum, but only the region between two consecutive minima.

F. Decompositions from Multiple ℓ s

In the case where two distinct anisotropy energy spectra, each measured at a different ℓ, can be obtained, a full decomposition is possible provided $\hat{C}_\ell$ varies with ℓ for at least one source class and $\hat{C}_{\ell,1}$ can be determined for each spectrum, e.g. via a plateau. We still assume $\hat{C}_\ell$ is independent of energy. Differentiating Eq. 3 with respect to energy and rearranging, we obtain,

$$\frac{d}{dE}\left(\frac{I_1}{I_{\rm tot}}\right) = \frac{d\hat{C}_{\ell,{\rm tot}}(E,\ell)/dE}{2\{\frac{I_1}{I_{\rm tot}}[\hat{C}_{\ell,1}(\ell) + \hat{C}_{\ell,2}(\ell)] - \hat{C}_{\ell,2}(\ell)\}} \quad (25)$$

Since the left-hand side is independent of ℓ, we must have for two different ℓ values ℓ_1 and ℓ_2 at *any* energy E

$$\frac{d\hat{C}_{\ell_1,{\rm tot}}/dE}{2[\frac{I_1}{I_{\rm tot}}(\hat{C}_{\ell_1,1} + \hat{C}_{\ell_1,2}) - \hat{C}_{\ell_1,2}]} = \quad (26)$$
$$\frac{d\hat{C}_{\ell_2,{\rm tot}}/dE}{2[\frac{I_1}{I_{\rm tot}}(\hat{C}_{\ell_2,1} + \hat{C}_{\ell_2,2}) - \hat{C}_{\ell_2,2}]}.$$

Using Eq. 3 to eliminate $\hat{C}_{\ell_1,2}$ and $\hat{C}_{\ell_2,2}$ and solving for I_1 yields

$$I_1 = I_{\rm tot}\frac{\hat{C}_{\ell_1,{\rm tot}}\frac{d\hat{C}_{\ell_2,{\rm tot}}}{dE} - \hat{C}_{\ell_2,{\rm tot}}\frac{d\hat{C}_{\ell_1,{\rm tot}}}{dE}}{\hat{C}_{\ell_1,1}\frac{d\hat{C}_{\ell_2,{\rm tot}}}{dE} - \hat{C}_{\ell_2,1}\frac{d\hat{C}_{\ell_1,{\rm tot}}}{dE}}. \quad (27)$$

This method is particularly ideal in that the input spectra are derived exactly and without making any assumptions about their relative intensities or anisotropies. However, this method may be difficult to implement for the IGRB because we expect most gamma-ray source populations to produce fluctuation angular power spectra that are dominated by the Poisson angular power, which takes the same value at all ℓ (e.g., [25, 31, 32, 58]), with the notable exception of dark matter annihilation or decay (e.g., [24, 32, 56, 59]).

V. THREE COMPONENT DECOMPOSITION

The separability of the equations for the total intensity and anisotropy at a given energy into contributions from each component source class enables a background of multiple components to be decomposed provided all source classes are uncorrelated and the contributions of all but two source classes are known. Furthermore, under certain conditions a decomposition can be performed even when information about additional source classes is more limited.

In this section, we discuss specifically the case of a three-component background. The intensity of a three component background as a function of energy is given by

$$I_{\rm tot} = I_1 + I_2 + I_3 \quad (28)$$

and the fluctuation anisotropy as a function of energy by

$$\hat{C}_{\ell,{\rm tot}}(E) = \left(\frac{I_1}{I_{\rm tot}}\right)^2 \hat{C}_{\ell,1} + \left(\frac{I_2}{I_{\rm tot}}\right)^2 \hat{C}_{\ell,2} + \left(\frac{I_3}{I_{\rm tot}}\right)^2 \hat{C}_{\ell,3} \quad (29)$$

again assuming uncorrelated components.

In the following, we examine the applicability of the techniques we discussed in two plausible scenarios for the IGRB composition.

A. One component with known intensity and anisotropy

It is possible that we can obtain, via some other analysis, expressions for both the intensity and anisotropy of a third component, I_3 and $\hat{C}_{\ell,3}$ as functions of energy. Such a situation could occur for a component arising from a population of (almost) uncorrelated bright point sources, for which enough individual members have been resolved so as to obtain a thorough understanding of the spectral behavior, and to constrain well the distribution of source fluxes, dN/dF, down to a point from which a reasonable extrapolation to even lower fluxes is possible. One can envision, for example, this to be the situation for gamma-ray blazars after the completion of the *Fermi* mission. From dN/dF both the anisotropy level and the overall intensity normalization can be calculated, and from the understanding of individual source spectra the energy dependence of the intensity can be evaluated.

We can thus rewrite our equations as

$$I_{\rm tot} - I_3 = I_1 + I_2 \quad (30)$$

and

$$\hat{C}_{\ell,{\rm tot}} - \left(\frac{I_3}{I_{\rm tot}}\right)^2 \hat{C}_{\ell,3} = \left(\frac{I_1}{I_{\rm tot}}\right)^2 \hat{C}_{\ell,1} + \left(\frac{I_2}{I_{\rm tot}}\right)^2 \hat{C}_{\ell,2}, \quad (31)$$

where the left hand side of both equations are determinable directly from observables and knowledge of the third component's properties. Hence, we have reduced the problem back to the two-component case where all of our decomposition methods apply.

B. One component with zero anisotropy, and a second component with known spectral shape

A second likely three-component scenario that is workable in this formalism is one in which no component is completely known, but where one component (component 1) has a well-understood and zero (or negligible) anisotropy, and a second component (component 2) has a

well-understood intensity spectral *shape*, even if its over-all intensity normalization is unknown.

In the context of the IGRB, the zero-anisotropy component could be contamination from unrejected cosmic-ray electrons entering the detector [20] or a combination of such cosmic-ray contamination and a very-low anisotropy cosmic component (e.g., star-forming galaxies, or cascade emission in the case of significant intergalactic magnetic field [60]). Blazars, on the other hand, could be the component with a well-understood spectral shape (since, by the end of the *Fermi* mission, thousands of blazars will have been resolved and have their individual spectra measured), even if the overall normalization of their intensity contribution to the IGRB is still uncertain.

We will see that in this case the energy dependence of the intensity of a third component can be determined up to a normalization constant. Such information could have extremely high impact if the third component (component 3) is, for example, a contribution from dark matter annihilation or decay, as we discuss in §VI.

Because component 1 has zero anisotropy, Eq. (31) becomes

$$\hat{C}_{\ell,\text{tot}}(E) = \left(\frac{I_2(E)}{I_{\text{tot}}(E)}\right)^2 \hat{C}_{\ell,2} + \left(\frac{I_3(E)}{I_{\text{tot}}(E)}\right)^2 \hat{C}_{\ell,3} \quad (32)$$

where we have written explicitly all energy dependencies.

We assume, as before, that there is an energy E_0 where we know that component 3 does not contribute significantly (as could be the case at low energies for certain dark matter annihilation or decay components). At E_0, Eq. (32) then becomes

$$I_{\text{tot}}^2(E_0)\hat{C}_{\ell,\text{tot}}(E_0) = I_2^2(E_0)\hat{C}_{\ell,2} . \quad (33)$$

Now since component 2 is assumed to have a known spectral shape, we can write

$$I_2(E) = I_2(E_0)g(E) \quad (34)$$

where $g(E)$ is a known function of energy, normalized so that $g(E_0) = 1$. Solving Eq. (32) for $I_3(E)$ and using Eqs. (33) and (34) to eliminate $\hat{C}_{\ell,2}$ and $I_2(E)$, we then obtain

$$I_3^2(E)\hat{C}_{\ell,3} = I_{\text{tot}}^2(E)\hat{C}_{\ell,\text{tot}}(E) - g^2(E)\hat{C}_{\ell,\text{tot}}(E_0)I_{\text{tot}}^2(E_0) . \quad (35)$$

Since all quantities on the right hand side of Eq. (35) are known, it follows that $I_3(E)$ can be derived up to a normalization constant $1/\sqrt{\hat{C}_{\ell,3}}$:

$$I_3(E) = \sqrt{\frac{I_{\text{tot}}^2(E)\hat{C}_{\ell,\text{tot}}(E) - g^2(E)\hat{C}_{\ell,\text{tot}}(E_0)I_{\text{tot}}^2(E_0)}{\hat{C}_{\ell,3}}} . \quad (36)$$

VI. DISCUSSION

Unraveling the contributions of multiple source classes to a diffuse background can be accomplished in many cases by combining intensity and anisotropy information. We have presented model-independent decomposition techniques which can recover the spectral shapes of the constituents of a two-component diffuse background (low-anisotropy plateau, known zero-anisotropy component) and techniques which can recover both the shape and normalization of the component spectra (double plateau, high-anisotropy plateau, minimum, multiple ℓ). Additionally, we have discussed cases in which these techniques can be applied to backgrounds of three or more components.

The techniques presented here are applicable at any wavelength and for any diffuse background composed of uncorrelated source classes (for example, in the case of the microwave background, the cosmic early-universe component, the dust emission from star-forming galaxies, and the contribution from blazars are uncorrelated or very weakly correlated components). Because each method has a clear signature in the observed anisotropy energy spectrum and/or straightforward mathematical tests of validity, there is no ambiguity in selecting which technique to apply. With the exception of the known zero-anisotropy component technique, no *a priori* assumptions need to be made about the nature of the component spectra. Hence, the methods presented here are unique and model-independent.

Each technique detailed in this paper, however, requires the source classes to have energy-independent fluctuation angular power, which is not a perfect assumption for many astrophysical sources, extragalactic ones in particular. Such a dependence would introduce degeneracy into the decompositions as any variations in the anisotropy energy spectrum could be explained either by changes in the fractional makeup of the intensity, as we have assumed here, or by changes in $\hat{C}_\ell$ with E for each source class. However, it is likely that these assumptions hold over at least some energy ranges. While in certain cases these methods can be applied to scenarios in which more than two components contribute to the diffuse emission, not all scenarios with three or more relevant contributors can be decomposed using the techniques presented here. Thus, a significant contribution from a third component in scenarios other than the two cases discussed in §V may render the application of these methods difficult at some energies.

The ability to decompose the intensity energy spectrum of the IGRB and recover the constituent spectra, even at an accuracy of up to a multiplicative constant, is of paramount importance in understanding the physical properties of the underlying source classes. Specifically in the case of blazars, the slope of their gamma-ray background contribution reveals the spectral properties of the unresolved blazar population [36] or the relative contribution of different type of blazars to gamma-ray background

and consequently to the faint end of the blazar luminosity function [6, 37]. If blazars are indeed a subdominant component of the gamma-ray background intensity, as suggested by recent constraints from the measured IGRB anisotropy [34, 35], such a decomposition would in principle allow us to deduce the slope of their collective emission at much higher accuracy than by modeling and subtracting the dominant components, the details of which may be largely unknown. In addition, a decomposed intensity spectrum for blazars can place constraints on the intensity of the EBL. In the case of dark matter, a decomposed intensity spectrum *is an uncontaminated measurement of the photon spectrum from dark matter annihilation or decay,* which in turn can provide information about the dark matter particle mass and dominant annihilation or decay channels.

At the same time, several of our techniques can constrain the source population anisotropy as well. Such constraints are also extremely important in understanding the statistical properties of a source class, as they provide information about the faint end of the luminosity function that is independent from that encoded by the collective intensity from unresolved members of the class.

Taken in complement with other analysis methods, these techniques can provide a unique, valuable window through which to probe the physics of the IGRB or any other diffuse astrophysical background.

[1] E. Komatsu et al. (WMAP Collaboration), Astrophys.J.Suppl. **192**, 18 (2011), 1001.4538.

[2] J. R. Primack, A. Domínguez, R. C. Gilmore, and R. S. Somerville, in *American Institute of Physics Conference Series*, edited by F. A. Aharonian, W. Hofmann, & F. M. Rieger (2011), vol. 1381 of *American Institute of Physics Conference Series*, pp. 72–83, 1107.2566.

[3] T. M. Kneiske and H. Dole, A&A **515**, A19 (2010), 1001.2132.

[4] F. W. Stecker, M. G. Baring, and E. J. Summerlin, Astrophys.J. **667**, L29 (2007), 0707.4676.

[5] A. M. Sołtan, A&A **475**, 837 (2007), 0709.2620.

[6] A. Abdo et al. (Fermi LAT Collaboration), Astrophys.J. **720**, 435 (2010), 1003.0895.

[7] K. N. Abazajian, S. Blanchet, and J. Harding, Phys.Rev. **D84**, 103007 (2011), 1012.1247.

[8] F. W. Stecker and T. M. Venters, Astrophys.J. **736**, 40 (2011), 1012.3678.

[9] B. D. Fields, V. Pavlidou, and T. Prodanovic, Astrophys.J. **722**, L199 (2010), 1003.3647.

[10] C.-A. Faucher-Giguere and A. Loeb, JCAP **1001**, 005 (2010), 0904.3102.

[11] P. Ullio, L. Bergstrom, J. Edsjo, and C. G. Lacey, Phys.Rev. **D66**, 123502 (2002), astro-ph/0207125.

[12] J. M. Overduin and P. Wesson, Phys.Rept. **402**, 267 (2004), astro-ph/0407207.

[13] G. Bertone, W. Buchmuller, L. Covi, and A. Ibarra, JCAP **0711**, 003 (2007), 0709.2299.

[14] J. C. Mather, E. Cheng, R. Shafer, C. Bennett, N. Boggess, et al., Astrophys.J. **354**, L37 (1990).

[15] D. Spergel et al. (WMAP Collaboration), Astrophys.J.Suppl. **148**, 175 (2003), astro-ph/0302209.

[16] A. W. Strong, I. V. Moskalenko, and O. Reimer, Astrophys.J. **613**, 956 (2004), arXiv:astro-ph/0405441.

[17] C. E. Fichtel, R. C. Hartman, D. A. Kniffen, D. J. Thompson, H. B. Ogelman, M. E. Ozel, and T. Tumer, ApJ **217**, L9 (1977).

[18] P. Sreekumar, D. L. Bertsch, B. L. Dingus, J. A. Esposito, C. E. Fichtel, R. C. Hartman, S. D. Hunter, G. Kanbach, D. A. Kniffen, Y. C. Lin, et al., Astrophys.J. **494**, 523 (1998).

[19] W. B. Atwood et al. (Fermi LAT Collaboration), Astrophys.J. **697**, 1071 (2009), 0902.1089.

[20] A. Abdo et al. (Fermi LAT Collaboration), Phys.Rev.Lett. **104**, 101101 (2010), 1002.3603.

[21] M. Ackermann et al. (Fermi LAT Collaboration), Phys.Rev. **D85**, 083007 (2012), 1202.2856.

[22] J. M. Siegal-Gaskins and V. Pavlidou, Phys.Rev.Lett. **102**, 241301 (2009), 0901.3776.

[23] P. Zhang and J. F. Beacom, Astrophys.J. **614**, 37 (2004).

[24] S. Ando and E. Komatsu, Phys. Rev. D **73**, 023521 (2006).

[25] S. Ando and V. Pavlidou, Mon.Not.Roy.Astron.Soc. **400**, 2122 (2009), 0908.3890.

[26] M. Ackermann, M. Ajello, A. Allafort, L. Baldini, J. Ballet, D. Bastieri, K. Bechtol, R. Bellazzini, B. Berenji, E. D. Bloom, et al., ApJ **755**, 164 (2012), 1206.1346.

[27] B. C. Lacki, S. Horiuchi, and J. F. Beacom, ArXiv e-prints (2012), 1206.0772.

[28] N. Chakraborty and B. D. Fields, ArXiv e-prints (2012),

1206.0770.

[29] F. W. Stecker and T. M. Venters, ApJ **736**, 40 (2011), 1012.3678.

[30] Y. Inoue, Astrophys.J. **733**, 66 (2011), 1103.3946.

[31] J. M. Siegal-Gaskins, R. Reesman, V. Pavlidou, S. Profumo, and T. P. Walker, Mon.Not.Roy.Astron.Soc. **415**, 1074S (2011), 1011.5501.

[32] S. Ando, E. Komatsu, T. Narumoto, and T. Totani, Phys.Rev. **D75**, 063519 (2007), astro-ph/0612467.

[33] Y. Inoue and T. Totani, Astrophys.J. **702**, 523 (2009), 0810.3580.

[34] A. Cuoco, E. Komatsu, and J. Siegal-Gaskins (2012), 1202.5309.

[35] J. P. Harding and K. N. Abazajian (2012), 1206.4734.

[36] V. Pavlidou and T. M. Venters, Astrophys.J. **673**, 114 (2008), 0710.0002.

[37] T. M. Venters and V. Pavlidou, Astrophys.J. **737**, 80 (2011), 1105.0372.

[38] A. A. Abdo et al. (Fermi LAT Collaboration), Astrophys.J. **723**, 1082 (2010).

[39] M. Georganopoulos, J. D. Finke, and L. C. Reyes, ApJ **714**, L157 (2010), 1004.0017.

[40] F. W. Stecker and S. T. Scully, Astrophys.J. **709**, L124 (2010), 0911.3659.

[41] J. D. Finke, S. Razzaque, and C. D. Dermer, Astrophys.J. **712**, 238 (2010), 0905.1115.

[42] A. Domínguez, J. R. Primack, D. J. Rosario, F. Prada, R. C. Gilmore, S. M. Faber, D. C. Koo, R. S. Somerville, M. A. Pérez-Torres, P. Pérez-González, et al., Mon.Not.Roy.Astron.Soc. **410**, 2556 (2011), 1007.1459.

[43] N. Fornengo, L. Pieri, and S. Scopel, Phys.Rev. **D70**, 103529 (2004), hep-ph/0407342.

[44] G. Jungman, M. Kamionkowski, and K. Griest, Phys.Rept. **267**, 195 (1996), hep-ph/9506380.

[45] G. Steigman, B. Dasgupta, and J. F. Beacom, Phys.Rev. **D86**, 023506 (2012), 1204.3622.

[46] M. Ackermann et al. (Fermi LAT collaboration), Phys.Rev.Lett. **107**, 241302 (2011), 1108.3546.

[47] A. Geringer-Sameth and S. M. Koushiappas, Phys.Rev.Lett. **107**, 241303 (2011), 1108.2914.

[48] I. Cholis and P. Salucci, Phys.Rev. **D86**, 023528 (2012), 1203.2954.

[49] M. Mazziotta, F. Loparco, F. de Palma, and N. Giglietto (2012), 1203.6731.

[50] M. Ackermann et al. (Fermi LAT Collaboration) (2012), 1205.6474.

[51] D. Hooper and T. Linden, Phys.Rev. **D84**, 123005 (2011), 1110.0006.

[52] D. Hooper, C. Kelso, and F. S. Queiroz (2012), 1209.3015.

[53] J. M. Siegal-Gaskins, JCAP **0810**, 040 (2008), 0807.1328.

[54] M. Fornasa, L. Pieri, G. Bertone, and E. Branchini, Phys.Rev. **D80**, 023518 (2009), 0901.2921.

[55] S. Ando, Phys.Rev. **D80**, 023520 (2009), 0903.4685.

[56] M. Fornasa, J. Zavala, M. A. Sanchez-Conde, J. M. Siegal-Gaskins, T. Delahaye, et al. (2012), 1207.0502.

[57] L. Knox, Phys.Rev. **D52**, 4307 (1995), astro-ph/9504054.

[58] F. Miniati, S. M. Koushiappas, and T. Di Matteo, Astrophys.J. **667**, L1 (2007), astro-ph/0702083.

[59] A. Cuoco, A. Sellerholm, J. Conrad, and S. Hannestad, Mon.Not.Roy.Astron.Soc. **414**, 2040 (2011), 1005.0843.

[60] T. M. Venters and V. Pavlidou (2012), 1201.4405.

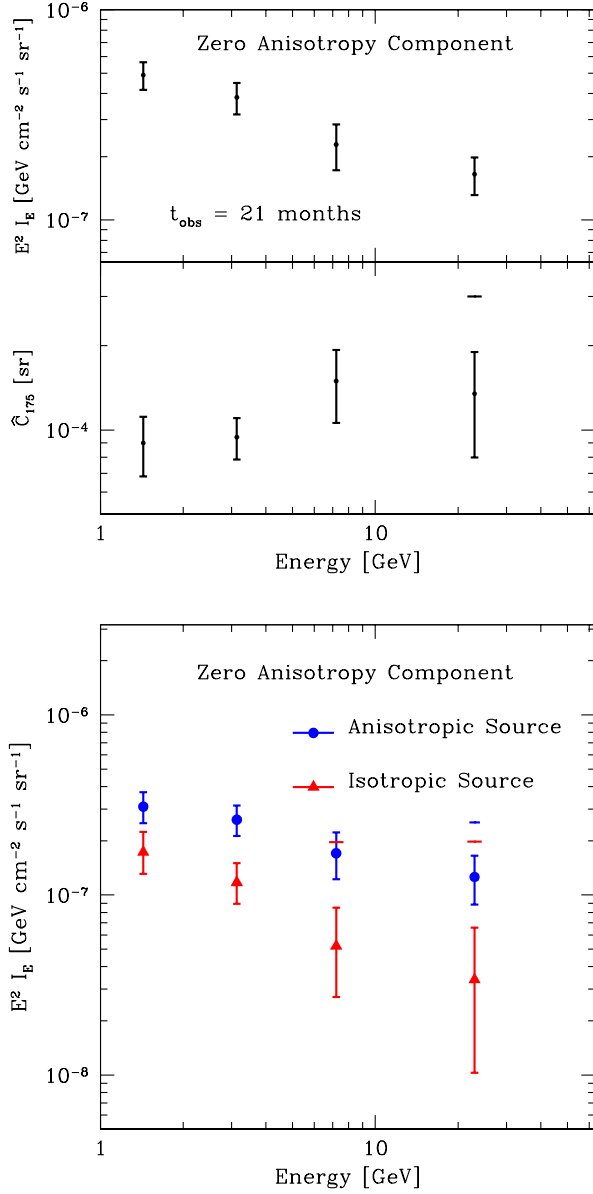[61] `http://www.slac.stanford.edu/exp/glast/groups/canda/lat_Per`

FIG. 4: Example known zero-anisotropy component decomposition. *Top:* Total IGRB intensity (top) and anisotropy (bottom) energy spectra as measured by *Fermi*-LAT using ∼ 21 months of data. If the data point is within 3σ of zero, we place a 3σ upper limit bar in addition to the 1σ error bars. Since the normalizations of the intensity spectra are not recovered with this technique, the spectra are shown with arbitrary normalization. *Bottom:* The decomposed intensity energy spectra of the anisotropic component (blue circles) and the zero-anisotropy component (red triangles) are recovered using the known zero-anisotropy component technique. Each component's input intensity spectrum is overlaid in black.